



## Accepted Article

**Title:** Analysing the Relation Between Structure and Aggregation Induced Emission (AIE) Properties of Iridium(III) Complexes through Modification of Non-Chromophoric Ancillary Ligands

**Authors:** Laura Abad Galán, David B. Cordes, Alexandra M.Z. Slawin, Denis Jacquemin, Mark I. Ogden, Massimiliano Massi, and Eli Zysman-Colman

This manuscript has been accepted after peer review and appears as an Accepted Article online prior to editing, proofing, and formal publication of the final Version of Record (VoR). This work is currently citable by using the Digital Object Identifier (DOI) given below. The VoR will be published online in Early View as soon as possible and may be different to this Accepted Article as a result of editing. Readers should obtain the VoR from the journal website shown below when it is published to ensure accuracy of information. The authors are responsible for the content of this Accepted Article.

**To be cited as:** *Eur. J. Inorg. Chem.* 10.1002/ejic.201801118

**Link to VoR:** <http://dx.doi.org/10.1002/ejic.201801118>

# Analysing the Relation Between Structure and Aggregation Induced Emission (AIE) Properties of Iridium(III) Complexes through Modification of Non-Chromophoric Ancillary Ligands

Laura Abad Galán<sup>a,b</sup> David B. Cordes<sup>b</sup>, Alexandra M.Z. Slawin<sup>b</sup>, Denis Jacquemin<sup>\*c</sup>, Mark I. Ogden<sup>\*a</sup>, Massimiliano Massi<sup>\*a</sup> and Eli Zysman-Colman<sup>\*b</sup>

**Abstract:** Unconventionally modified dibenzoylmethane (dbm) ligands have been synthesised and successfully utilised as ancillary ligands for neutral Ir(III) complexes of the formula [Ir(dFppy)<sub>2</sub>(LX)], where dFppyH is 2-(2,4-difluorophenyl)pyridine and LX is tribenzoylmethane (t<sub>3</sub>bm) or 1-phenyl-3-(4-(pyridin-2-yl)phenyl)propane-1,3-dione (pydbm). The modification of the ligands aims to prevent or enhance possible intermolecular interactions between the dFppy and/or the LX moiety in comparison with the previously reported [Ir(dFppy)<sub>2</sub>(dbm)] complex. The aggregation induced emission (AIE) properties of these complexes are significantly modulated, as a consequence of the different π-π interactions revealed by X-ray crystallography.

## Introduction

Since the observation of phosphorescence of tris(2,2'-bipyridyl)ruthenium(II) dichloride [Ru(bpy)<sub>3</sub>]Cl<sub>2</sub>,<sup>1</sup> phosphorescent transition metal complexes have garnered a great deal of attention<sup>2-6</sup> due to their use in a wide range of applications such as emitters for electroluminescent devices,<sup>7</sup> sensitizers for energy and electron transfer,<sup>8-11</sup> photocatalysis,<sup>6,12-15</sup> dyes for solar cells,<sup>16</sup> imaging reagents as biological probes,<sup>17-19</sup> and sensors.<sup>20,21</sup>

Aggregation-induced emission (AIE) is a photophysical phenomenon, first formulated in 2001, where non-emissive luminogens are induced to emit light after the formation of aggregates.<sup>22</sup> Its discovery provided a new platform of research that quickly motivated the science community because of its potential application particularly in life science and biomedical engineering.<sup>23-27</sup> Solid-state phosphorescence emission, sometimes described as AIE, has been often found in platinum (II) complexes. Owing to their planar structures, Pt-Pt interactions in the solid state are possible, allowing efficient metal-metal-to-ligand charge transfer (MMLCT) transitions.<sup>28-30</sup> In contrast, octahedral iridium complexes cannot interact in a similar manner, making MMLCT transitions impossible. In 2008, the first AIE iridium(III) complex was presented, [Ir(ppy)<sub>2</sub>(dbm)],

where ppyH = 2-phenylpyridine and dbm = dibenzoylmethane.<sup>31</sup>

This complex showed strong π-π interactions between the offset pyridine rings of two adjacent ppy ligands with a distance of ~3.37 Å. This proximity modifies the nature of the excited states, presenting enhanced phosphorescence in the solid state. Since then numerous examples have been presented in the literature.<sup>32-37</sup> Moreover, several examples of dFppy-based iridium complexes have also shown AIE properties.<sup>35,38-40</sup> The [Ir(dFppy)<sub>2</sub>(dbm)] complex [dFppyH = 2-(2,4-difluorophenyl)pyridine], in particular, presented different π-π interactions between two neighbouring complexes in the X-ray structure that involved the dFppy and the ancillary dbm ligands. However, the lack of examples where structural organisation and AIE effects are directly compared inspired us to undertake this study. Two new complexes and the previously reported complex [Ir(dFppy)<sub>2</sub>(dbm)], which is used as reference, have been synthesised in an effort to better understand the relationship between intermolecular interactions, particularly involving the ancillary ligand, and the AIE phenomenon. The dFppy ligand was chosen as the cyclometalating moiety as it is known to favor π-π interactions in the solid state. Firstly, the previously reported dbm and t<sub>3</sub>bm<sup>41</sup> molecules were employed as ancillary ligands to probe if the extra carbonyl group on the α-CH position would inhibit the π-π interactions between the phenyl rings of the dbm moiety. Secondly, two new molecules, 1-phenyl-3-(4-(pyridin-2-yl)phenyl)propane-1,3-dione (pydbmH) and 2-benzoyl-1-phenyl-3-(4-(pyridin-2-yl)phenyl)propane-1,3-dione (pyt<sub>3</sub>bmH) were designed to assess the effect of the extra pyridine ring, which could potentially allow intermolecular interactions in a similar manner to the dFppy moiety.

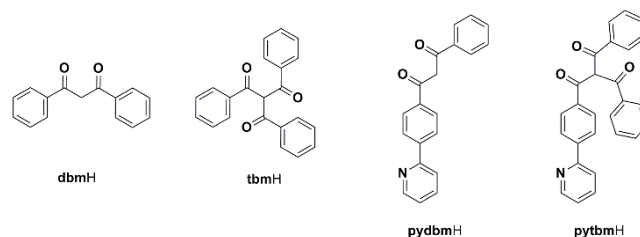


Figure 1. Structures of the ancillary ligands used in this report.

## Results and Discussion

**Synthesis of ligands.** The 1-phenyl-3-(4-(pyridin-2-yl)phenyl)propane-1,3-dione (pydbmH) was synthesised in two steps via a Claisen condensation to afford the intermediate 1-(4-bromophenyl)-3-phenylpropane-1,3-dione (Br-dbmH) in 85% yield, followed by a Stille cross-coupling reaction in 40% yield to obtain the desired molecule. The 2-benzoyl-1-phenyl-3-(4-(pyridin-2-yl)phenyl)propane-1,3-dione molecule (pyt<sub>3</sub>bmH) was obtained by reaction of the pydbmH and benzoylchloride

<sup>a</sup> Laura Abad Galán, Prof. Mark I. Ogden and Asoc. Prof. Max Massi, School of Life and Molecular Science and Curtin Institute for Functional Molecules and Interfaces, Curtin University, Kent Street, Bentley 6102 WA, Australia.

<sup>b</sup> Laura Abad Galán, David D. Cordes, Prof. Alexandra M.Z. Slawin and Reader Eli Zysman-Colman, Organic Semiconductor Centre, EaStCHEM School of Chemistry, University of St. Andrews, St. Andrews, Fife, KY16 9ST, United Kingdom

<sup>c</sup> Prof. Denis Jacquemin, School of CEISAM, UMR CNRS 6230, University of Nantes, 2 rue de la Houssinière, 44322 Nantes, France.

\*E-mail: [m.massi@curtin.edu.au](mailto:m.massi@curtin.edu.au); [m.ogden@curtin.edu.au](mailto:m.ogden@curtin.edu.au); [Denis.Jacquemin@univ-nantes.fr](mailto:Denis.Jacquemin@univ-nantes.fr); [eli.zysman-colman@st-andrews.ac.uk](mailto:eli.zysman-colman@st-andrews.ac.uk)

† Electronic Supplementary Information (ESI) available: See DOI: 10.1039/x0xx00000x

(Figure 2) in 65% yield. Both ligands were characterised by melting point,  $^1\text{H-NMR}$ ,  $^{13}\text{C-NMR}$  spectroscopy, mass spectrometry and elemental analysis (See experimental section).

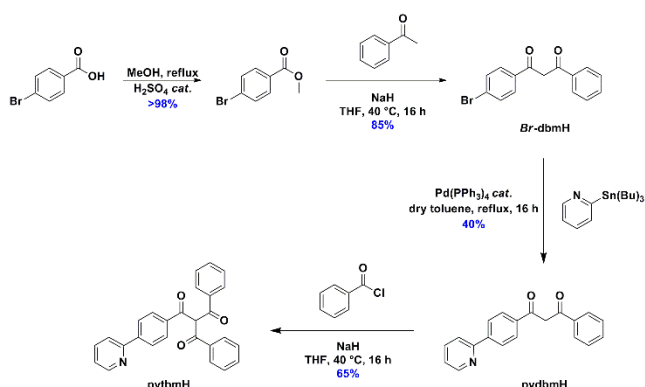


**Figure 2.** Reaction scheme for ligands **pydbmH** and **pytbmH**.

**Synthesis of the complexes.** The chloro-bridged dimer,  $[\text{Ir}(\text{dFppy})_2(\mu\text{-Cl})_2]$ , was synthesised in 67% yield by refluxing dFppyH in 2-ethoxyethanol with  $\text{IrCl}_3$  as the iridium source. For the synthesis of the previously reported complex  $[\text{Ir}(\text{dFppy})_2(\text{dbm})]$  (**1**), sodium carbonate in 2-ethoxyethanol was used, affording the product in 90% yield, where the characterisation matched that previously reported.<sup>42</sup> When this methodology was followed for the synthesis of **2** using **tbmH**, the resulting retro-Claisen condensation product, **1**, was obtained. However, when triethylamine in a mixture of DCM/EtOH (80:20 v/v) was employed, the desired complex **2** was isolated in 40% yield; the retro-Claisen product **1** corresponded to the remainder of the isolated material in a 30% yield (Figure 3).

The synthesis of **3'** was first attempted without the presence of base in 2-ethoxyethanol. These conditions were chosen to favor the coordination of the **pydbm** in a C<sup>N</sup> mode leaving the  $\beta$ -diketone moiety free for further coordination. However, the crystal structure of the resulting purified product, obtained in 50% yield, showed coordination of the ligand in a ketonate mode within the complex  $[\text{Ir}(\text{dFppy})_2(\text{pydbm})]$ , **3** (Figure 4b). The conditions of the complexation reaction were then modified in an attempt to increase the yield of the reaction. When  $\text{NEt}_3$  and a mixture of DCM/EtOH (80:20 v/v) were used, complex **3** was synthesised

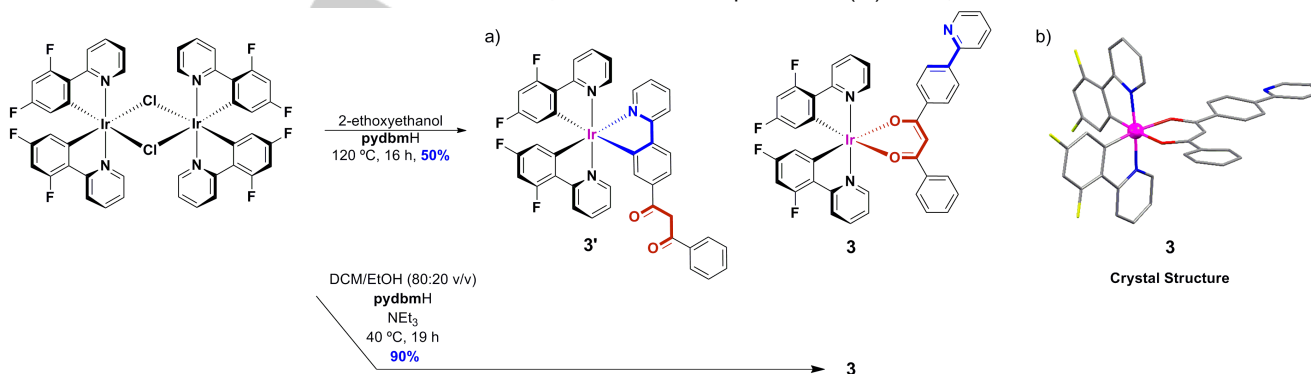


**Figure 4.-** Reaction scheme for complexes **3'** and **3**.

in an excellent yield of 90%. Finally, the synthesis of complex **4**,  $[\text{Ir}(\text{dFppy})_2(\text{pytbm})]$ , was attempted following the O<sup>^</sup>O coordination conditions. Unfortunately, the desired complex could not be isolated and only the retro-Claisen condensation complex, **3**, was obtained as the main product of the reaction in 80% yield. Retro-Claisen condensation reactions of  $\beta$ -triketones in solution has been previously noted<sup>43,44</sup> by us and the scope and mechanism of this transformation is currently under investigation. The three isolated complexes **1-3** were fully characterised by melting point,  $^1\text{H-NMR}$ ,  $^{13}\text{C-NMR}$ ,  $^{19}\text{F-NMR}$ , mass spectrometry and elemental analysis (see experimental section).

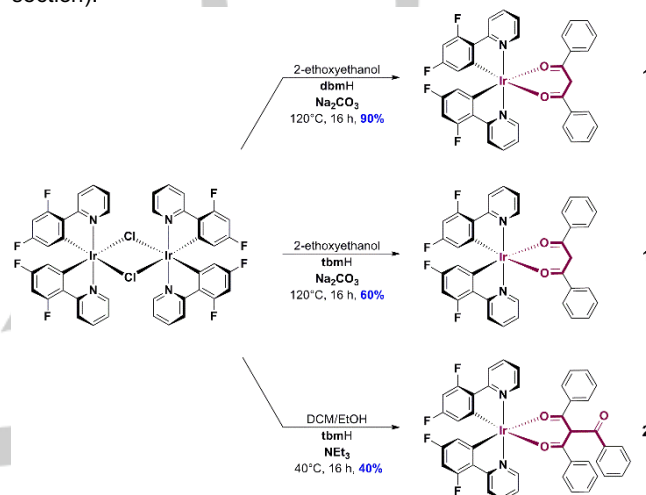


**Figure 3.** Reaction scheme for complexes **1** and **2**.

**X-ray diffraction studies.** The crystal structure of **1** had already been reported. The literature report stated that the  $[\text{Ir}(\text{dFppy})_2(\text{dbm})]$  complex crystallised as two polymorphs: one in the space group  $C2/c$  and the other one in  $P\bar{1}$ .<sup>38</sup> The main difference between the two is the presence of different  $\pi$ - $\pi$  interactions between two neighbouring complexes, involving a combination of two dFppy, one dFppy and one dbm or two dbm ligands.

In the case of complexes **2** and **3**, crystals were obtained from dichloromethane by slow diffusion of either ether (**2**) or hexane (**3**). Complex **3** crystallised in the triclinic space group  $P\bar{1}$ . The asymmetric unit contained two similar but symmetrically inequivalent Ir(III) units, with an Ir...Ir distance of 8.85 Å.

Interestingly, these two independent Ir(III) complexes are connected by  $\pi$ - $\pi$  interactions involving the offset pyridine group of a dFppy ligand and the phenyl ring of the pendant phenylpyridine moiety of **pydbm**, with interplanar distance and centroid-to-centroid distance of 3.315 Å and 3.808 Å, respectively (**Error! Reference source not found.**).

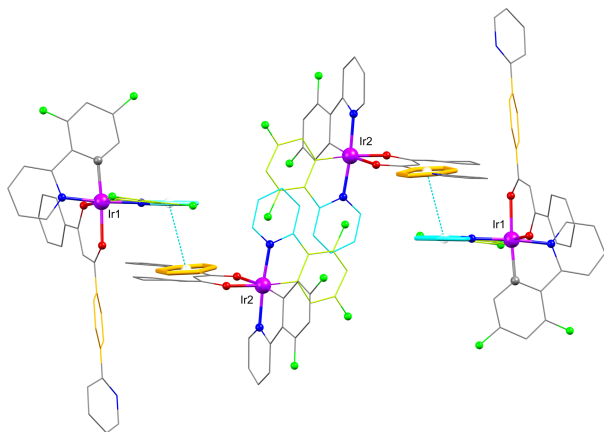


**Figure 5.** Representation of the X-ray crystal structure of  $[\text{Ir}(\text{dFppy})_2(\text{pydbm})]$  (**3**), emphasising the supramolecular composition formed by  $\pi$ - $\pi$  stacking interactions. Hydrogen atoms and solvent molecules have been omitted for clarity.

In the case of **2**, the complex crystallised in the monoclinic space group  $I2/a$ , with a single complex in the asymmetric unit. Only one set of  $\pi$ - $\pi$  interaction are found (**Error! Reference source not found.**); between adjacent and offset dFppy ligands, with a centroid to centroid distance of 3.678(2) Å. This  $\pi$ - $\pi$  interaction also has a pair of  $\text{CH}\cdots\pi$  interactions working in concert with it, involving hydrogen atoms on the  $\pi$ -stacking rings interacting with the  $\pi$ -system of further dFppy rings of the adjacent complex, at a distance of 2.62 Å. As predicted, the extra acyl group of the  $\beta$ -triketionate, in comparison to the **dbm** molecule, seems to be responsible of the lack of  $\pi$ - $\pi$  interactions between the phenyl rings of two subsequent units. However, weak  $\text{C-H}\cdots\text{O}$  hydrogen bonds do occur, between a phenyl C-H of a coordinated ketone, and the non-coordinating ketone oxygen of an adjacent complex ( $\text{CH}\cdots\text{O}$  distance of 2.57 Å, corresponding  $\text{C}\cdots\text{O}$  separation of 3.234(4) Å). These interactions give rise to a weakly interacting zigzag chain running along the crystallographic  $b$ -axis.

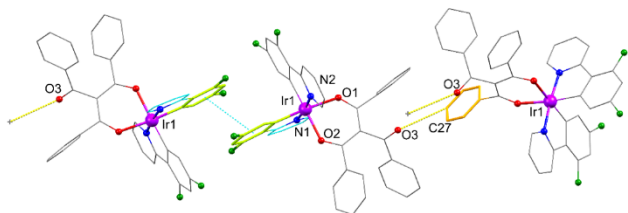


**Figure 6.** Representation of the X-ray crystal structure of  $[\text{Ir}(\text{dFppy})_2(\text{tbm})]$  (**2**), emphasising the supramolecular structure formed by intermolecular interactions. Hydrogen atoms and molecules of solvent have been omitted for clarity.

**UV-VIS absorption.** The absorption spectra of **1-3** measured in acetonitrile are presented in **Error! Reference source not found.** while Figure S13 provides the corresponding spectra obtained with Time-Dependent Density Functional Theory (TD-DFT). Complexes **2** and **3** present relatively unstructured spectra comparable to that of **1**, which itself shows a profile equivalent to that reported in the literature.<sup>38</sup> Complexes **2** and **3** show higher molar absorptivities compared to **1**, likely due to the presence of the extra acyl group and pyridine ring, respectively, in these complexes. The high energy absorption bands are assigned to  $\pi$ - $\pi^*$  transitions of the dFppy<sup>45,46</sup> and ancillary ligands.<sup>31,47</sup> (250 - 350 nm). The low energy band at 380 nm is attributed to a metal-to-ligand charge transfer transition (<sup>1</sup>MLCT), while bands above 400 nm can be assigned to mixed CT.<sup>38</sup> The onset of the CT bands is of comparable energy at  $\sim 465$  nm for the three complexes, which suggests that these bands are based on the  $\pi$  orbitals of the dFppy ligands and similar metal orbitals. TD-DFT predicts the lowest vertical singlet transitions at 413 ( $f=0.02$ ) and 406 nm ( $f=0.04$ ), 409 ( $f=0.02$ ) and 406 nm ( $f=0.03$ ), and 426 ( $f=0.01$ ) and 407 nm ( $f=0.04$ ) for **1**, **2** and **3**, respectively, all of which correspond to mixed HOMO to LUMO and HOMO to LUMO+1 transitions. As can be seen in Figure S14, the HOMO is localised on the metal and fluorinated phenyl rings, whereas the LUMO and LUMO+1 are localised on the ancillary ligand and C<sup>N</sup> ligands, respectively. These bands therefore have a mixed MLCT and LLCT character.

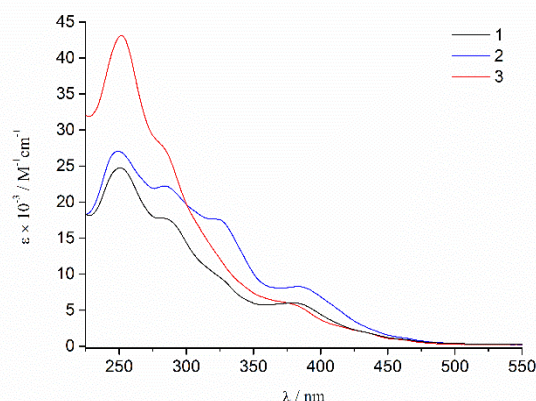


**Figure 7.** Absorption spectra of  $[\text{Ir}(\text{dFppy})_2(\text{L})]$  for  $\text{L} = \text{dbm}$  (black trace), **tbm** (blue trace) and **pydbm** (red trace) in acetonitrile at room temperature (ca.  $10^{-5}$  M).

**Electrochemistry.** The electrochemical properties were studied by cyclic voltammetry (CV) and differential pulse voltammetry (DPV) in de-aerated MeCN at 298 K in order to estimate the energies of the frontier molecular orbitals of **1-3**. A summary of the redox potentials of the complexes, referenced with respect to the saturated calomel electrode, SCE, ( $\text{Fc}/\text{Fc}^+ = 0.38$  V in MeCN)<sup>48</sup>, is given in Table 1.

The electrochemistry of the related tris-cyclometalated Ir(III) complex, *fac*- $\text{Ir}(\text{dFppy})_3$ , had been previously studied.<sup>49</sup> The reversible oxidation of this reference complex involves the

iridium ion and the  $\pi$  orbitals of the difluorophenyl (dFph) part of the **dFppy** ligands ( $\text{Ir}^{\text{III/IV}} + \text{dFph}$ ) whereas the reduction is localised on the pyridyl ring of the **dFppy** ligands. Thus, if oxidation or reduction processes involving the ancillary ligand do not take part in these systems, complexes **1-3** will present a comparable behaviour to that of  $\text{fac-Ir}(\text{dFppy})_3$ . The reported redox values for  $\text{fac-Ir}(\text{dFppy})_3$  are  $E_{\text{ox}} = 0.76 \text{ V}$ ;  $E_{\text{red}} = -2.49 \text{ V}$  vs SCE in MeCN. A second reference complex,  $[\text{Ir}(\text{dFppy})_2(\text{acac})]$ ,<sup>50</sup> possesses comparable electrochemical properties ( $E_{\text{ox}} = 0.76 \text{ V}$ ;  $E_{\text{red}} = -2.44 \text{ V}$  vs SCE) to those of  $\text{fac-Ir}(\text{dFppy})_3$ .

The oxidation potentials of **1-3** were found, respectively, at 1.05 V, 1.30 V and 1.10 V (Figure 8). These numbers vary significantly from the oxidation potentials for the two reference complexes, suggesting some contribution from the ancillary ligands, likely via influence of the electron density on the iridium. Furthermore, while **1** and **3** show similar oxidation potentials, complex **2** presents a larger value, which is indicative of a stronger influence of **tbm** in comparison to **dbm** or **pydbm** on the oxidation process. When looking at the reduction potential values ( $E_{\text{red}}(\mathbf{1}) = -1.85 \text{ V}$ ;  $E_{\text{red}}(\mathbf{2}) = -1.67 \text{ V}$ ;  $E_{\text{red}}(\mathbf{3}) = -1.60 \text{ V}$ ) a significant change with respect to the reduction of  $\text{fac-Ir}(\text{dFppy})_3$  ( $E_{\text{red}} = -2.49 \text{ V}$ ) is observed that is indicative of an ancillary ligand-based LUMO, in agreement with previous assignments in the literature for the  $[\text{Ir}(\text{dFppy})_2(\text{dbm})]$ ,<sup>38,42</sup> as well as with the present theoretical result (Figure S14).

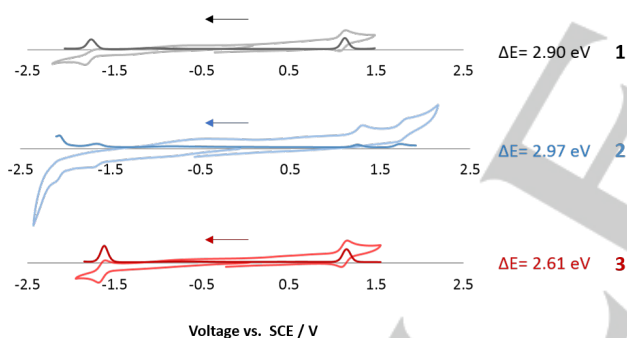


**Figure 8.** CV and DPV traces of **1** (black trace), **2** (red trace) and **3** (blue trace), versus SCE ( $\text{Fc}/\text{Fc}^+ = 0.38 \text{ V}$  in MeCN). Scan rates of  $100 \text{ mV s}^{-1}$  with scans taken in the negative direction.

Surprisingly, significantly different values of the oxidation and reduction potentials as well as the redox gap were found in the literature for **2** ( $E_{\text{ox}}^{42} = 0.32 \text{ V}$ ,  $E_{\text{red}}^{42} = -2.02 \text{ V}$  and  $\Delta E^{42} = 2.34 \text{ eV}$ ;  $E_{\text{ox}}^{38} = 0.73 \text{ V}$ ,  $E_{\text{red}}^{38} = -2.16 \text{ V}$  and  $\Delta E^{38} = 2.64 \text{ eV}$ ).<sup>38,42</sup> These literature values are also different to the experimental data observed in the present study under similar conditions ( $E_{\text{ox}}(\mathbf{1}) = 1.05 \text{ V}$ ,  $E_{\text{red}}(\mathbf{1}) = -1.85 \text{ V}$  and  $\Delta E(\mathbf{1}) = 2.90 \text{ eV}$ ). This could be due to different values given for the internal standard ferrocene/ferrocenium ( $\text{Fc}/\text{Fc}^+$ ).<sup>48</sup> While in the case reported here a value of  $0.38 \text{ V}$  vs SCE<sup>48</sup> was used, other numbers such as  $0.40 \text{ V}$ <sup>51</sup> or  $0.45 \text{ V}$ <sup>52</sup> can also be found in literature. Unfortunately, the reported literature for complex **2** does not include the number used for this referencing, making this comparison infeasible.

The LUMO of complex **3** is the most stabilised, which is a logical consequence of the presence of a pyridyl ring. The DFT calculation indeed also return a LUMO more stabilised in **3** than in both **1** and **2**, by  $-0.16 \text{ eV}$ . As can be seen in the ESI, the LUMO of **1** and **3** is localised almost exclusively on the ancillary ligand, whereas there is additionally a small contribution from the C<sup>N</sup> ligand for **2**.

**Table 1.** Electrochemical data for complexes **1-3**.<sup>a</sup>

Complex	$E_{\text{ox}}/\text{V}^b$	HOMO/ $\text{eV}^c$	$E_{\text{red}}/\text{V}^b$	LUMO/ $\text{eV}^c$	$\Delta E_{\text{H-L}}/\text{eV}$
$\text{fac-Ir}(\text{dFppy})_3$ <sup>49</sup>	0.76	-5.56	-2.49	-2.31	3.25
$\text{Ir}(\text{dFppy})_2(\text{acac})$ <sup>50</sup>	0.76	-5.56	-2.44	-2.36	3.20
<b>1</b>	1.05	-5.85	-1.85	-2.95	2.90
<b>2</b>	1.30	-6.10	-1.67	-3.13	2.97
<b>3</b>	1.10	-5.81	-1.60	-3.20	2.61

<sup>a</sup>. Measurements were performed in MeCN at 298 K at a scan rate of  $100 \text{ mV s}^{-1}$ , with  $\text{Fc}/\text{Fc}^+$  used as an internal standard. <sup>b</sup>. Potential values were obtained from the DPV spectra and referenced with respect to SCE ( $\text{Fc}/\text{Fc}^+ = 0.38 \text{ V}$ ).<sup>48</sup> <sup>c</sup>. The energies of the HOMO and LUMO levels estimated using:  $E_{\text{HOMO}} = -[E_{\text{ox vs Fc/Fc}^+} + 4.8] \text{ eV}$  and  $E_{\text{LUMO}} = -[E_{\text{red vs Fc/Fc}^+} + 4.8] \text{ eV}$ , respectively.

**Photophysics.** The photophysical properties of **1-3** were studied in MeCN and dichloromethane at room temperature, in a dichloromethane frozen matrix at 77 K, in doped films (10 wt% in PMMA) and in the solid state as powder samples. The photophysical data, including excited state lifetimes ( $\tau_{\text{PL}}$ ) and photoluminescence quantum yields ( $\Phi_{\text{PL}}$ ) are reported in **Error! Reference source not found.** and **3**.

The room temperature emission spectra in deaerated MeCN show very weak emission at 629 nm, 498 nm and 625 nm for the **1**, **2** and **3**, respectively (Figure 9). In the case of complexes **1** and **3**, the broad emission band is significantly red-shifted compared to the structured emission of  $\text{fac-Ir}(\text{dFppy})_3$  at 469 nm, itself previously assigned to mixed MLCT/LC transitions.<sup>49</sup> The  $\tau_{\text{PL}}$  were found to be on the order of nanoseconds ( $\tau_{\text{PL}}(\mathbf{1}) = 12 \text{ ns}$  and  $\tau_{\text{PL}}(\mathbf{3}) = 7.5 \text{ ns}$ ) and the  $\Phi_{\text{PL}}$  values below 1%, indicative of large non-radiative decay. This photophysical profile strongly contrasts with the  $\Phi_{\text{PL}}$  and  $\Phi_{\text{PL}}$  of  $\text{fac-Ir}(\text{dFppy})_3$  ( $\tau_{\text{PL}} = 1.64 \mu\text{s}$ ,  $\Phi_{\text{PL}} = 77\%$ )<sup>49</sup>. Indeed, previous DFT calculations for **1** suggested that the emission had MLCT mixed with intraligand charge transfer (ILCT) character and the poor emissive properties in solution were caused by efficient non-radiative decay promoted by strong vibrations of the **dbm** in the low frequency region.<sup>53</sup> Therefore, comparable behaviour would be expected for complex **3**. In the case of complex **2**, although the emission maximum is not significantly shifted with respect to the <sup>3</sup>MLCT/LC transition of  $\text{fac-Ir}(\text{dFppy})_3$ , the  $\tau_{\text{PL}}$  (30 ns),  $\Phi_{\text{PL}}$  (2%) and profile of the emission bands are indicative of significant changes and seem more characteristic of significantly quenched ligand-centred (LC) emission. For **1**, **2** and **3**, the DFT computed 0-0 phosphorescence wavelengths are 565, 518 and 576 nm, respectively, which should correspond to the intersection point between the absorption and phosphorescence bands. The ordering is in good agreement with the measurements of Figure

**9**, although our value for **2** is too blue-shifted. Therefore, the triplet states of the three ancillary ligands were also estimated at the 0-0 transition of the phosphorescence spectra of their gadolinium complexes. Values of 487 nm, 183 nm and 504 nm for the **dbm**, **tbm** and **pydbm** were found, respectively (Figure S15). In the case of **tbm**, this experimental value matches with what it was observed for complex **2**, which confirms the LC nature of this transition.

The evolution of the geometry of the structures in going from the lowest singlet to triplet states (coordinates in the ESI) is also markedly different. While for **2**, the acac moiety is almost unaffected by the change of state, in both **1** and **3**, one notices a shortening of the Ir-O bonds (from ca. 2.16 Å to 2.09 Å) and a significant change of dihedral angle of the acac moiety compared to the ideal orientation that goes from 2-3° in the singlet state to ca. 25° in the triplet state. The computed spin density difference plots can be found in Figure 10. For **1** and **3** the spin density of the triplet is mainly localised on the metal and the ancillary ligands, hence explaining the similarity between the two emission spectra. In contrast, in **2**, the triplet state is mainly localised on one of the two more rigid C^N ligands according to DFT, consistent with the emission profile shown in Figure 9 as well as with the above described changes of structures. It is also interesting to note that the spin density on the Ir centre is estimated to be similar in all three complexes (ca. 0.5-0.6), i.e., it is the localisation of the triplet rather than the involvement of the metal that differs in the three structures.

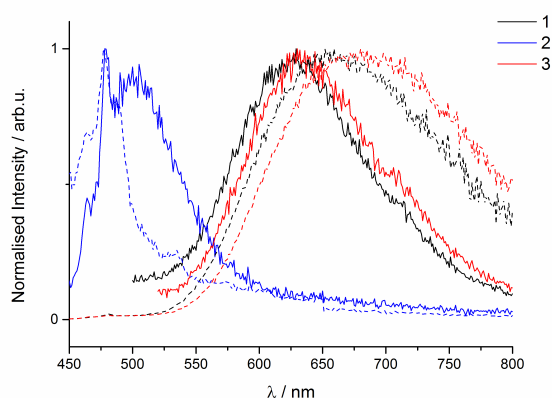


**Figure 9.** Normalised emission ( $\lambda_{\text{exc}} = 420$  nm) spectra for **1** (black trace), **2** (blue trace) and **3** (red trace) in MeCN (solid trace) and dichloromethane at room temperature (ca.  $10^{-5}$  M) (dashed trace).

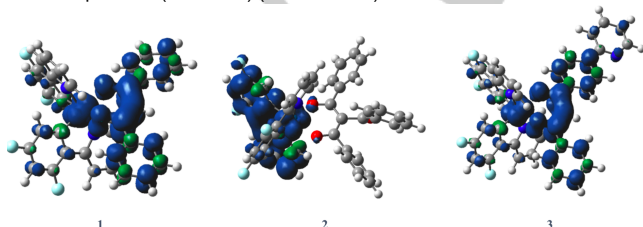


**Figure 10.** Spin density difference plots for the lowest triplet states of the three studied complexes, where the contour threshold for the spin density is  $2 \times 10^{-3}$  au.

The photoluminescence spectra were also studied in deaerated dichloromethane at room temperature in order to assess the impact of using less polar solvents (Figure 9). CT states are frequently found to be stabilised upon increasing the solvent polarity.<sup>54-58</sup> This effect is commonly known as positive solvatochromism. However, solvatochromism is a complex phenomenon as many different interactions and dynamic processes can take place. Indeed, the experimental data for complexes **1** and **3** showed an unusual but not unprecedented<sup>59,60</sup> negative solvatochromic shift. This indicates a decrease of the dipole moment in the excited state with respect to the ground state, i.e., DFT predicts that the total dipole moment of **1** (**3**) goes from 6.8 to 1.2 D (6.8 to 3.2 D) when going from the ground to the excited state. Such changes naturally translates into a higher stabilisation of the ground state in more polar solvents consistently with previous suggestions.<sup>59</sup> By contrast, the emission maximum undergoes a slight positive solvatochromism in complex **2**, which is consistent with DFT (increase of dipole from 5.4 D to 8.9 D) and with the different nature of the triplet state (*vide supra*).<sup>45</sup>

When the photoluminescence properties were studied in a frozen dichloromethane matrix, a clear blue-shift was identified in complexes **1** and **3**, while the emission maximum of **2** remained unchanged (Figure 11). The fact that no rigidochromic shift was found for the emission maximum in **2** hints to a <sup>3</sup>LC nature emission for this complex in the solid-state. By contrast, the blue-shifted emission of complexes **1** and **3** suggests mixed CT character, in agreement with the literature and the RT PL studies.<sup>42</sup> The three complexes in the frozen matrix presented prolonged lifetime values of 800 ns, 3.77 μs and 630 ns for **1**, **2** and **3**, respectively. These longer lifetimes can be explained by a reduction of the vibrational motions at 77 K, which results in a decrease in the non-radiative decay rate. While **1** and **3** have similar  $\Phi_{\text{PL}}$  values, that of **2** is much longer, which is another indication that in this case, the transition is LC in nature.

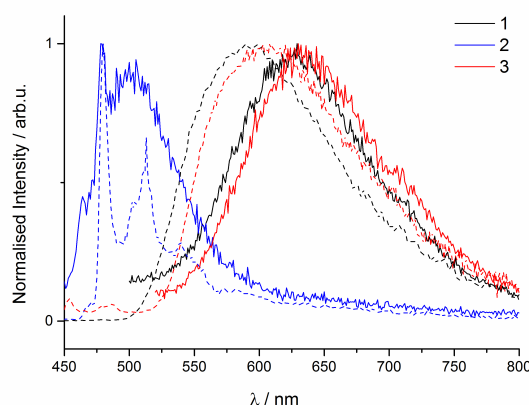


**Figure 11.** Normalised emission ( $\lambda_{\text{exc}} = 420$  nm) spectra for **1** (black trace), **2** (blue trace) and **3** (red trace) in MeCN ( $10^{-5}$  M) at room temperature (dark trace) and in a dichloromethane matrix at 77 K (dashed trace).

In contrast to the weak emission found for the three complexes in solution, intense luminescence was produced at ~550 nm when the complexes were doped into films (10 wt% in PMMA), with improved photoluminescence quantum yields of 8.2%, 8.9% and 6.3% for **1**, **2** and **3**, respectively (Figure 12). As previously observed for [Ir(dFppy)<sub>2</sub>(dbm)] (**1**),<sup>38,42</sup> the phosphorescence mechanism for **2** and **3** is modulated by intermolecular interactions. These interactions promote the stabilisation of the excited states and also induce reduced non-radiative decay. Interestingly, the maximum emission wavelength is similar for the three complexes at ~550 nm, which may indicate that the transitions occurring are based on similar delocalised states as previously suggested for **1**.<sup>31</sup>

**Table 2.** Photophysical data of **1-3** in MeCN and DCM (ca. 10<sup>-5</sup> M) at RT and 77 K.

Complex	Medium	$\lambda_{PL}$ / nm	$\Phi_{PL}$ / % <sup>a</sup>	$\tau_{PL}$ / ns
<b>1</b>	MeCN-RT	629	1.02	12
	DCM-RT	660	-	18
	DCM-77K	595	-	800
<b>2</b>	MeCN-RT	498	2.1	2 (35%), 30 (65%)
	DCM-RT	477	-	17
	DCM-77K	478	-	3770
<b>3</b>	MeCN-RT	625	0.5	7.5
	DCM-RT	679	-	10
	DCM-77K	607	-	630

<sup>a</sup> Photoluminescence quantum yields in MeCN relative to [Ru(bpy)<sub>3</sub>](PF<sub>6</sub>)<sub>2</sub> in MeCN ( $\Phi_{PLref} = 9.5\%$ )<sup>61</sup>

When the photophysical behaviour of **1-3** were explored in the crystalline powder state, where there can be different sets of intermolecular interactions, a red-shift in the emission maximum was found for each of the here investigated complexes (Figure 12). These data suggest that the excited states change nature due to the different intermolecular interactions as a function of increased aggregation. Interestingly, the largest shift was found for complex **2**, which happened to present the strongest ancillary ligand-based interactions as assessed by the relatively shorter distance of 3.2 Å, against 3.4 Å for the **dbm** and **pydbm** ligands in the crystal structure. Photoluminescence quantum yields and excited state lifetimes in the powder state were measured to be 21%, 3% and 6%, and 361 ns, 13 ns and 97 ns for **1**, **2** and **3**, respectively. These data reveal that the **dbm**-containing complexes are more efficient emitters in the powder. Indeed, while radiative decay rates ( $k_r$ ), calculated from  $\Phi_{PL} = k_r / (k_r + k_{nr})$  were comparable for complexes **1** and **3** and significantly larger in the case of **2**, non-radiative decay rates ( $k_{nr}$ ) for **2** and **3** were found to be 30 and 4 times larger than that of **1** ( $22 \cdot 10^6 \text{ s}^{-1}$ ). It is important to note that the plane of the acac unit for complexes **1** and **3** in the excited state is significantly distorted with respect to the C-Ir-C plane while this distortion is almost negligible for complex **2**. These data therefore suggest that the lack of distortion in the solid state may lead to possible deactivation pathways, which is in agreement with results previously found on acac and iminophenolate complexes.<sup>62</sup>

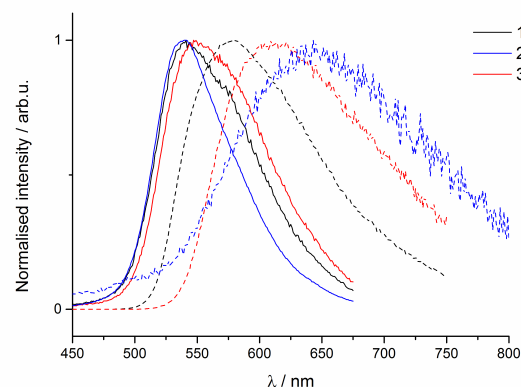


**Figure 12.** Normalised emission spectra ( $\lambda_{exc} = 420 \text{ nm}$ ) for **1** (black trace), **2** (blue trace) and **3** (red trace) in doped films (10 wt% in PMMA) (solid trace) and as powder (dashed trace).

**Table 3.** Photophysical data of **1-3** in PMMA doped films and powder ( $\lambda_{exc} = 420 \text{ nm}$ ).

Complex	Medium	$\lambda_{PL}$ / nm	$\Phi_{PL}$ / % <sup>a</sup>	$\tau_{PL}$ / ns	$k_r \times 10^{-6}$ / s <sup>-1</sup>	$k_{nr} \times 10^{-6}$ / s <sup>-1</sup>
<b>1</b>	Film <sup>b</sup>	542	8.2	3 (71%)	-	-
				140	-	-
				425	-	-
<b>2</b>	Film <sup>b</sup>	542	8.9	1 (34%)	-	-
				3 (37%)	-	-
				11 (28%)	-	-
<b>3</b>	Film <sup>b</sup>	550	6.3	4 (33%),	-	-
				116	-	-
				358	-	-
<b>3</b>	Powder	612	5.9	26%	6.20	97.21
				97	-	-
				97	-	-

<sup>a</sup> Photoluminescence quantum yields measured with an integrating sphere. <sup>b</sup> Films were prepared by doping 10 wt% of the complex in PMMA.

As a function of this analysis, AIE studies were performed on **1-3**. Indeed, addition of water into dilute acetonitrile solutions turned on the photoluminescence emission of the three complexes with a large enhancement in the emission intensity for **3**, a modest enhancement for **1**, and almost a negligible effect for the **tbm** analogue, **2** (Figures 13, S11 and S12, respectively). These results clearly suggest that the structural modifications of the ancillary ligands tune the intermolecular interactions, and hence directly affect the AIE behaviour. The PL intensity was a maximum when the water content reached 70%, 80% and 60% for **1**, **2** and **3**, respectively, and then decreased at higher percentages in every case. This is probably due to two different reasons: firstly, after aggregation, the molecules become covered with other aggregated particles and do not emit light;<sup>63</sup>

and secondly, because in the process of aggregation of crystallites, amorphous particles are simultaneously formed, which do not enhance the emission intensity.<sup>64</sup>

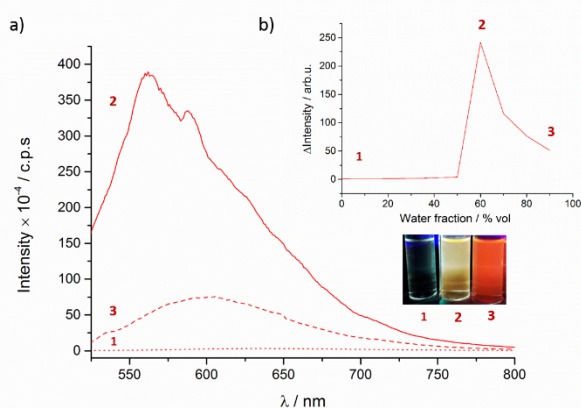


**Figure 13.** a) Emission spectra ( $\lambda_{exc} = 420$  nm) of **3** in dilute MeCN (1) MeCN-H<sub>2</sub>O (4:6 v/v) (2) and MeCN-H<sub>2</sub>O (1:9 v/v) (3). b) Variation of intensity according to water content.

## Conclusions

Herein, two novel iridium complexes, [Ir(dFppy)<sub>2</sub>(pydbm)], **3**, and [Ir(dFppy)<sub>2</sub>(tbm)], **2**, bearing  $\beta$ -diketonate/triketone ligands, respectively, were synthesised and their optoelectronic properties compared to the reference complex [Ir(dFppy)<sub>2</sub>(dbm)], **1**. All three complexes are poorly emissive in acetonitrile and dichloromethane solutions while their emission properties are remarkably enhanced in both 10 wt% PMMA films and as powders. By analysing the molecular packing in the crystal structures of **2** and **3**, the aggregation-induced emission could be explained by a change in the nature of the emission to one based on a mixed metal-to-ligand charge transfer and ligand-to-ligand charge transfer state formed in the solid state. These results showed that the addition of different substituents to the dbm moiety, a pyridyl group in the case of [Ir(dFppy)<sub>2</sub>(pydbm)], or a benzoyl group in the case of [Ir(dFppy)<sub>2</sub>(tbm)], alters the  $\pi$ - $\pi$  stacking involving the ancillary ligands and disrupts the intermolecular interactions of the cyclometalated moiety (dFppy), which modulates the AIE properties of the iridium complexes.

## Experimental Section

**General Procedures.** Commercial chemicals were used as supplied. All reactions were carried out using solvents of reagent grade or better. Flash column chromatography was performed using silica gel (60 Å, 40–63  $\mu$ m). Analytical thin layer chromatography (TLC) was performed using silica plates with aluminum backings (250  $\mu$ m with indicator F-254). Compounds were visualised under UV light. <sup>1</sup>H, <sup>13</sup>C and <sup>19</sup>F NMR spectra were recorded on Bruker Avance spectrometers at 300 – 500 MHz, 126 MHz and 376 MHz, respectively. High-resolution mass spectra were recorded at the EPSRC UK National Mass

Spectrometry Facility at Swansea University on a quadrupole time-of-flight (ESI-Q-TOF), model ABSciex 5600 Triple TOF in positive electrospray ionisation mode and spectra were recorded using sodium formate solution as the calibrant. Elemental analyses were performed by Mr. Stephen Boyer, London Metropolitan University. Melting points (Mp) were recorded using open-ended capillaries on an Electrothermal melting point apparatus and are uncorrected.

**Photophysical measurements.** All samples were prepared in HPLC grade MeCN. Absorption spectra were recorded at room temperature using a Shimadzu UV-1800 double beam spectrophotometer. Molar absorptivity determination was verified by linear least squares fit of values obtained from at least four independent solutions at varying concentrations ranging from  $5.22 \times 10^{-5}$  to  $8.41 \times 10^{-6}$  M. The sample solutions for the emission spectra were prepared in HPLC grade MeCN and degassed via three freeze–pump–thaw cycles using an in-house designed quartz cuvette. Steady-state and time-resolved emission spectra were recorded at room temperature using a Gilden photonics Fluorimeter and Edinburgh Instruments FLS980 fluorimeter, respectively. For steady-state measurements at room temperature complexes **1–3** were excited at 420 nm. The excited state lifetimes of the complexes were obtained by time correlated single photon counting (TCSPC) at an excitation wavelength of 378 nm using a pulsed diode laser, and PL emission was detected at the corresponding steady-state emission maximum for each complex. Photoluminescence quantum yields in solution were determined using the optically dilute method.<sup>65</sup> A stock solution with absorbance of ca. 0.2 was prepared, and then four dilutions were prepared with dilution factors between 2 and 20 to obtain solutions with absorbances of ca. 0.103, 0.076, 0.052, and 0.026, respectively. The Beer–Lambert law was found to be respected (linear dependency) at the concentrations of the solutions. The emission spectra were then measured after the solutions were degassed by three freeze–pump–thaw cycles using an in-house designed quartz cuvette prior to spectrum acquisition. For each sample, linearity between absorption and emission intensity was verified through linear regression analysis, and additional measurements were acquired until the Pearson regression factor ( $R^2$ ) for the linear fit of the data set surpassed 0.9. Individual relative quantum yield values were calculated for each solution, and the values reported represent the slope value. The  $\Phi_s = \Phi_r(A_r/A_s)(I_s/I_r)(n_s/n_r)^2$  equation was used to calculate the relative quantum yield of each of the sample, where  $\Phi_r$  is the absolute quantum yield of the reference,  $n$  is the refractive index of the solvent,  $A$  is the absorbance at the excitation wavelength, and  $I$  is the integrated area under the corrected emission curve. The subscripts  $s$  and  $r$  refer to the sample and reference, respectively. A solution of [Ru(bpy)<sub>3</sub>](PF<sub>6</sub>)<sub>2</sub> in deaerated MeCN at 298 K ( $\Phi_{PL} = 9.5\%$ ) was used as a reference.<sup>61</sup> Quantum yields in the solid state were measured with the use of an integrating sphere coated with BenFlect.<sup>66</sup>

**Electrochemical measurements.** Cyclic voltammetry (CV) and differential pulse voltammetry (DPV) measurements were

performed on an Electrochemical Analyzer potentiostat model 600D from CH Instruments. Solutions were prepared in MeCN and degassed with solvent-saturated nitrogen by bubbling for ca. 10 min prior to scanning. Tetra(*n*-butyl)ammoniumhexafluorophosphate (TBAPF<sub>6</sub>; ca. 0.1 M in MeCN) was used as the supporting electrolyte. Two Ag/Ag<sup>+</sup> electrodes (silver wire in a solution of 0.1 M KCl in H<sub>2</sub>O) were used as the pseudoreference electrode and counter electrode, respectively; a platinum electrode was used for the working electrode. The redox potentials are reported relative to a saturated calomel electrode (SCE) electrode with a ferrocene/ferrocenium (Fc/Fc<sup>+</sup>) redox couple as the internal reference (0.38 V vs SCE).<sup>48</sup>

**Theoretical methods.** To perform DFT and TD-DFT calculations, we have used the Gaussian16 program.<sup>67</sup> Our calculations consisted in geometry optimisation vibrational spectra determinations and TD-DFT calculations of the different structures. We have applied default procedures, integration grids, algorithms and parameters, except for tighten energy (typically 10–10 a.u.) and internal forces (10–5 a.u.) convergence thresholds. The ground-state geometrical parameters have been determined with the M06 functional.<sup>68</sup> The vibrational spectrum has been subsequently determined analytically at the same level of theory and it has been checked that all structures correspond to true minima of the potential energy surface. At least, the first thirty low-lying excited-states have been determined within the vertical TD-DFT approximation using the same functional, that is suited for optical spectra.<sup>69,70</sup> Phosphorescence was studied by optimizing the lowest triplet excited-state with unrestricted DFT (M06 functional). For the structural and vibrational calculations, we used the LanL2DZ atomic basis set and pseudo-potential for all atoms, augmented by d functions with  $\alpha=0.587, 0.736, 0.961$  and  $1.577$  for C, N, O and F, respectively and f functions with exponent of  $0.938$  for the Ir centres. During all steps, a modelling of bulk solvent effects (here CH<sub>3</sub>CN) through the Polarizable Continuum Model (PCM),<sup>71</sup> using the liner-response approach in its non-equilibrium limit for the TD-DFT part of the calculation. The contour threshold used to draw the MOs (spin densities) was set to  $0.02$  ( $0.002$ ) au.

### Synthesis of ligands

**pydbmH** (1-phenyl-3-(4-(pyridin-2-yl)phenyl)propane-1,3-dione). 4-bromo benzoic acid (1 g, 4.90 mmol, 1.2 equiv.) was dissolved in MeOH in the presence of a catalytic amount of H<sub>2</sub>SO<sub>4</sub> and refluxed for 16 h. The crude mixture was then neutralised with saturated Na<sub>2</sub>CO<sub>3</sub> and extracted with ethyl acetate (3 x 15 mL). The organic layer was then dried under reduced pressure giving the correspondent methyl 4-bromobenzoate as a white solid in a quantitative yield. A suspension of NaH (60% in mineral oil, 468 mg, 11.70 mmol, 3 equiv.) was prepared in 15 mL of THF and stirred for 30 min. at 0 °C. After this time, a solution of the acetophenone (465 mg, 3.90 mmol, 1 equiv.) in 7 mL of THF was added dropwise at 0 °C. The same step was then performed with the previously prepared methyl 4-bromobenzoate (1 g, 4.65 mmol, 1.2 equiv.). The suspension was kept at room temperature for 1 h. and then heated at 40 °C for

16 more h. The crude mixture was neutralised with an HCl solution (1 M) and extracted with ethyl acetate (3 x 15 mL). The compound was purified by recrystallisation from EtOH giving a white solid corresponding to 1-(4-bromophenyl)-3-phenylpropane-1,3-dione (Br-dbmH) in 85% yield, whose characterisation matched with reported literature.<sup>72</sup> Finally, 2-(tributylstannyl)pyridine (607 mg, 1.65 mmol, 1 equiv.) was reacted with the previously formed Br-dbmH (500 mg, 1.65 mmol, 1 equiv.) using Stille coupling reaction conditions catalysed by Pd(PPh<sub>3</sub>)<sub>4</sub> (92 mg, 0.08 mmol, 0.05 equiv.) in dry toluene.<sup>73</sup> The reaction mixture was refluxed for 32 h. at 120 °C. The crude product was purified by silica gel chromatography (hexanes/ethyl acetate 90:10.), giving the pure compound as a light brown solid. Yield 40%.  $R_f = 0.55$ . M.p. 83–85 °C. <sup>1</sup>H NMR (500 MHz, CDCl<sub>3</sub>)  $\delta$  8.77 (dt,  $J = 4.7, 1.4$  Hz, 1H), 8.15 (q,  $J = 8.6$  Hz, 4H), 8.07 – 8.02 (m, 2H), 7.86 – 7.80 (m, 2H), 7.63 – 7.57 (m, 1H), 7.56 – 7.50 (m, 2H), 7.33 (ddd,  $J = 6.2, 4.8, 2.6$  Hz, 1H), 6.95 (s, 1H). <sup>13</sup>C NMR (126 MHz, CDCl<sub>3</sub>)  $\delta$  186.13, 184.88, 156.16, 149.93, 143.06, 135.71, 135.59, 132.54, 128.72, 127.65, 127.40, 127.12, 122.89, 120.97, 93.36, 77.28, 77.03, 76.77. HR-MS (FTMS<sup>+</sup>) [M+H]<sup>+</sup>: Calculated: 302.1176, Found: 302.1209. Elemental analysis calcd (%) for C<sub>20</sub>H<sub>15</sub>NO<sub>2</sub>(H<sub>2</sub>O): C, 77.40; H, 5.20; N, 4.51; found: C, 77.80; H, 5.35 H, 4.27.

**pytbmH** (2-benzoyl-1-phenyl-3-(4-(pyridin-2-yl)phenyl)propane-1,3-dione). NaH (60% in mineral oil, 40 mg, 0.99 mmol, 3 equiv.) and pydbmH (100 mg, 0.33 mmol, 1 equiv.) were combined in 10 mL of THF and the suspension was maintained at 0 °C. To this suspension, the benzoyl chloride (93 mg, 0.66 mmol, 2 equiv.) in 5 mL of THF was added dropwise. After the addition, the mixture was stirred under a nitrogen atmosphere at 40 °C for 24 h. The crude was neutralised with an acetic acid solution (1 M) and extracted with ethyl acetate (3 x 10 mL). The organic layers were dried under vacuum and the resulting solid washed with diethyl ether in order to remove the excess of benzoic acid formed in the reaction mixture. The pure compound resulted as a pale brown solid. Yield: 50%. M.p. 197–199 °C. <sup>1</sup>H NMR (400 MHz, CDCl<sub>3</sub>)  $\delta$  8.81 – 8.67 (m, 1H), 8.17 – 8.01 (m, 4H), 8.01 – 7.93 (m, 4H), 7.84 – 7.76 (m, 2H), 7.63 (t,  $J = 7.4$  Hz, 2H), 7.50 (t,  $J = 7.7$  Hz, 4H), 7.32 (ddd,  $J = 6.6, 4.8, 1.7$  Hz, 1H), 7.19 (s, 1H). <sup>13</sup>C NMR (101 MHz, CDCl<sub>3</sub>)  $\delta$  192.03, 191.71, 136.17, 135.69, 134.06, 129.54, 129.39, 129.05, 128.80, 128.49, 128.31, 128.12, 127.69, 114.98, 66.50. HR-MS (FTMS<sup>+</sup>) [M+H]<sup>+</sup>: Calculated: 406.1435, Found: 406.1438. Elemental analysis calcd (%) for C<sub>27</sub>H<sub>19</sub>O<sub>3</sub> (0.75·H<sub>2</sub>O): C, 77.40; H, 4.93; N, 3.34; found: C, 77.40; H, 4.57; N, 3.35.

### Synthesis of complexes

**[Ir(dFppy)<sub>2</sub>( $\mu$ -Cl)]<sub>2</sub>** (Tetrakis[2-(4',6'-difluorophenyl)-pyridinato-N,C2']-bis( $\mu$ -chloro)diiridium(III)). A modified version of the originally reported by Nonoyama was followed.<sup>74</sup> IrCl<sub>3</sub>·3H<sub>2</sub>O (1 equiv.) and the C<sup>\*</sup>N ligand (2.2 equiv.) were dissolved in 2-ethoxyethanol and distilled water (3:1 v/v) to give a concentration of ca. 0.2 M. The mixture was degassed by three cycles of vacuum/ N<sub>2</sub> and heated to reflux for 18 h. After 1 h. a yellow precipitate was observed. The reaction was cooled to room temperature follow by addition of water to favor the

precipitation of the dimer. The isolated solid was washed with a mixture of water and ethanol (1:1 v/v) and then a mixture of hexanes and diethyl ether (1:1 v/v), before drying to give the title compound. Tetrakis[2-(4',6'-difluorophenyl)-pyridinato-N,C2']-bis( $\mu$ -chloro)diiridium(III),  $[\text{Ir}(\text{dFppy})_2(\mu\text{-Cl})_2]$ . Yield: 67%.  $^1\text{H-NMR}$  (400 MHz,  $\text{CDCl}_3$ ) ( $\delta$ ) 9.12 (d,  $J = 6.7$  Hz, 1H), 8.31 (d,  $J = 9.3$  Hz, 1H), 7.87 – 7.78 (m, 1H), 6.83 (t,  $J = 7.2$  Hz, 1H), 6.38 – 6.31 (m, 1H), 5.29 (d,  $J = 9.1$  Hz, 1H).  $^{19}\text{F-NMR}$  (377 MHz,  $\text{CDCl}_3$ ) ( $\delta$ ) -107.72 (d,  $J = 10.3$  Hz), -110.32 (d,  $J = 10.3$  Hz). The characterisation matched with reported literature.<sup>74</sup>

**General procedure for the synthesis of  $[\text{Ir}(\text{dFppy})_2(\text{L})]$ .** To a round bottom flask containing  $[\text{Ir}(\text{dFppy})_2(\mu\text{-Cl})_2]$  (100 mg, 0.08 mmol) and the LH (LH = **dbmH**, **tbmH**, **pydbmH** and **pytbmH**) (0.18 mmol, 2.2 equiv.) and  $\text{NEt}_3$  (0.18 mmol, 1 equiv.) were added in a mixture DCM/MeOH (80:20 v/v) to give a suspension with a concentration of ca. 0.02 M. The mixture was degassed via bubbling with  $\text{N}_2$  for 10 min, before the reaction vessel was sealed. The reaction mixture was heated to 40 °C for 19 h. The solution was cooled to room temperature, and the solvent evaporated. The crude product was purified by silica gel chromatography in hexanes/DCM (70:30), giving in each case the pure compound as a yellow solid.

$[\text{Ir}(\text{dFppy})_2(\text{dbm})]$  (**1**). Yield: 90%.  $R_f = 0.43$ . M.p. 307-309 °C.  $^1\text{H-NMR}$  (500 MHz,  $\text{DMSO-}d_6$ )  $\delta$  8.50 (dd,  $J = 6.0, 1.5$  Hz, 2H), 8.26 (d,  $J = 8.5$  Hz, 2H), 8.06 – 8.01 (m, 1H), 7.85 – 7.77 (m, 4H), 7.54 – 7.43 (m, 4H), 7.39 (t,  $J = 7.7$  Hz, 4H), 6.76 (ddd,  $J = 12.2, 9.4, 2.4$  Hz, 2H), 6.71 (s, 1H), 5.65 (dd,  $J = 8.7, 2.4$  Hz, 2H).  $^{19}\text{F-NMR}$  (470 MHz,  $\text{DMSO-}d_6$ )  $\delta$  -108.88, -110.64 (d,  $J = 9.9$  Hz). The characterisation matched with reported literature.<sup>42</sup>

$[\text{Ir}(\text{dFppy})_2(\text{tbm})]$  (**2**). Yield: 40%.  $R_f = 0.67$ . M.p. 317-319 °C.  $^1\text{H-NMR}$  (500 MHz,  $\text{CDCl}_3$ )  $\delta$  8.52 (d,  $J = 5.8$  Hz, 2H), 8.26 (d,  $J = 8.3$  Hz, 2H), 7.76 (m,  $J = 17.1, 8.2$  Hz, 6H), 7.43 (t,  $J = 7.3$  Hz, 2H), 7.33 (t,  $J = 7.6$  Hz, 4H), 7.10 (t,  $J = 7.3$  Hz, 2H), 6.59 (s, 1H), 6.39 (ddd,  $J = 11.7, 9.4, 2.4$  Hz, 2H), 5.77 (dd,  $J = 8.8, 2.3$  Hz, 2H).  $^{19}\text{F-NMR}$  (471 MHz,  $\text{CDCl}_3$ )  $\delta$  -108.52 – -108.68 (m), -110.69 – -110.88 (m).  $^{13}\text{C-NMR}$  (126 MHz,  $\text{CDCl}_3$ )  $\delta$  186.24, 148.06, 138.46, 129.44, 129.11, 127.71, 127.04, 77.28, 77.03, 76.77, 65.89. HR-MS (TOFMS<sup>+</sup>)  $[\text{M}+\text{H}]^+$ : Calculated: 901.1668, Found: 901.1673. Elemental analysis calcd (%) for  $\text{C}_{44}\text{H}_{27}\text{O}_3\text{N}_2\text{Ir}$ : C, 58.73; H, 3.02; N, 3.11; found: C, 58.74; H, 3.12; N, 3.12.

$[\text{Ir}(\text{dFppy})_2(\text{pydbm})]$  (**3**). Yield: 90%.  $R_f = 0.25$ . M.p. 313-315 °C.  $^1\text{H-NMR}$  (500 MHz,  $\text{CDCl}_3$ )  $\delta$  8.72 (d,  $J = 4.3$  Hz, 1H), 8.57 (t,  $J = 4.9$  Hz, 2H), 8.29 (d,  $J = 8.2$  Hz, 2H), 8.03 – 7.86 (m, 4H), 7.86 – 7.70 (m, 6H), 7.42 (dt,  $J = 51.5, 7.5$  Hz, 3H), 7.14 (ddt,  $J = 7.5, 5.9, 1.6$  Hz, 2H), 6.67 (s, 1H), 6.42 (ddt,  $J = 12.4, 9.3, 3.0$  Hz, 2H), 5.80 (dt,  $J = 8.7, 2.9$  Hz, 2H).  $^{19}\text{F-NMR}$  (377 MHz,  $\text{CDCl}_3$ )  $\delta$  -109.13 (dd,  $J = 9.9, 4.6$  Hz), -111.33 (dd,  $J = 10.1, 3.2$  Hz).  $^{13}\text{C-NMR}$  (126 MHz, Chloroform-*d*)  $\delta$  207.07, 179.39, 178.63, 165.28, 163.59, 161.69, 159.75, 156.64, 151.56, 149.85, 148.02, 140.95, 138.00, 130.60, 128.77, 127.33, 126.89, 122.52, 121.76, 120.69, 115.18, 97.25, 95.20. HR-MS (FTMS<sup>+</sup>)  $[\text{M}+\text{H}]^+$ : Calculated: 874.1669, Found: 874.1664. Elemental analysis calcd (%) for

$\text{C}_{42}\text{H}_{26}\text{O}_2\text{N}_3\text{Ir}$ : C, 57.59; H, 3.00; N, 4.81; found: C, 57.78; H, 2.91; N, 5.00.

### X-Ray Crystallography

X-ray diffraction data for both complexes were collected at 173 K using a Rigaku FR-X Ultrahigh Brilliance Microfocus RA generator/confocal optics with XtaLAB P200 diffractometer [Mo  $\text{K}\alpha$  radiation ( $\lambda = 0.71075$  Å)]. Intensity data were collected using  $\omega$  steps accumulating area detector images spanning at least a hemisphere of reciprocal space. Data for all compounds analysed were collected and processed (including correction for Lorentz, polarisation and absorption) using CrystalClear.<sup>75</sup> Structures were solved by Patterson methods (PATTY)<sup>76</sup> and refined by full-matrix least-squares against  $F^2$  (SHELXL-2018/3).<sup>77</sup> Non-hydrogen atoms were refined anisotropically, and hydrogen atoms were refined using a riding model. All calculations were performed using the CrystalStructure interface.<sup>78</sup> Selected crystallographic data are presented in Table S1. CCDC 1849982-1849983 contains the supplementary crystallographic data for this paper. The data can be obtained free of charge from The Cambridge Crystallographic Data Centre via [www.ccdc.cam.ac.uk/structures](http://www.ccdc.cam.ac.uk/structures).

### Acknowledgments

E.Z.-C. acknowledges the University of St. Andrews and EPSRC (EP/M02105X/1) for financial support. We thank Umicore AG for the gift of materials. We thank the EPSRC UK National Mass Spectrometry Facility at Swansea University for analytical services. This work is supported by a Royal Society International Exchanges Grant and by the Australian Research Council and. LAG thanks Curtin University for the postgraduate scholarship. This work used the computational resources of the CCIPL installed in Nantes.

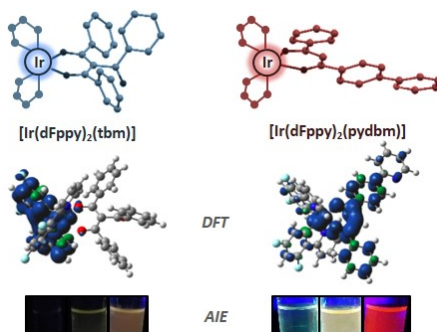
**Keywords:** Iridium • AIE •  $\beta$ -triketones •

- 1 J. P. Paris and W. W. Brandt, *J. Am. Chem. Soc.*, 1959, **81**, 5001–5002.
- 2 I. M. Dixon, J.-P. Collin, J.-P. Sauvage, L. Flamigni, S. Encinas and F. Barigelletti, *Chem. Soc. Rev.*, 2000, **29**, 385–391.
- 3 A. F. Henwood and E. Zysman-Colman, *Chem. Commun.*, 2017, **53**, 807–826.
- 4 J. A. Gareth Williams, S. Develay, D. L. Rochester and L. Murphy, *Coord. Chem. Rev.*, 2008, **252**, 2596–2611.
- 5 V. W.-W. Yam and K. M.-C. Wong, *Chem. Commun.*, 2011, **47**, 11579–11592.
- 6 C. K. Prier, D. A. Rankic and D. W. C. MacMillan, *Chem. Rev.*, 2013, **113**, 5322–5363.
- 7 R. D. Costa, E. Orti, H. J. Bolink, F. Monti, G. Accorsi and N. Armaroli, *Angew. Chemie - Int. Ed.*, 2012, **51**, 8178–8211.
- 8 D. Sykes and M. D. Ward, *Chem. Commun.*, 2011, **47**, 2279–81.
- 9 J. R. Piper, L. Cletheroe, C. G. P. Taylor, A. J. Metherell, J. A. Weinstein, I. V. Sazanovich and M. D. Ward, *Chem. Commun.*, 2017, **53**, 408–411.
- 10 D. Sykes, A. J. Cankut, N. M. Ali, A. Stephenson, S. J. P.

- Spall, S. C. Parker, J. a Weinstein and M. D. Ward, *Dalton Trans.*, 2014, **43**, 6414–28.
- 11 H. Tsubaki, A. Sekine, Y. Ohashi, K. Koike, H. Takeda and O. Ishitani, *J. Am. Chem. Soc.*, 2005, **127**, 15544–15555.
- 12 J. H. Montoya, L. C. Seitz, P. Chakthranont, A. Vojvodic, T. F. Jaramillo and J. K. Nørskov, *Nat. Mater.*, 2016, **16**, 70–81.
- 13 J. J. Concepcion, J. W. Jurss, M. K. Brennaman, P. G. Hoertz, A. O. T. Patrocinio, N. Y. Murakami Iha, J. L. Templeton and T. J. Meyer, *Acc. Chem. Res.*, 2009, **42**, 1954–1965.
- 14 J. W. Tucker and C. R. J. Stephenson, *J. Org. Chem.*, 2012, **77**, 1617–1622.
- 15 G. Sahara, R. Abe, M. Higashi, T. Morikawa, K. Maeda, Y. Ueda and O. Ishitani, *Chem. Commun.*, 2015, **51**, 10722–10725.
- 16 M. K. Nazeeruddin and M. Gratzel, *Photofunctional Transition Metal Complexes*, 2007, vol. 123.
- 17 A. J. Amoroso, M. P. Coogan, J. E. Dunne, V. Fernández-Moreira, J. B. Hess, A. J. Hayes, D. Lloyd, C. Millet, S. J. A. Pope and C. Williams, *Chem. Commun.*, 2007, **29**, 3066–3068.
- 18 K. K. W. Lo, M. W. Louie and K. Y. Zhang, *Coord. Chem. Rev.*, 2010, **254**, 2603–2622.
- 19 C. Caporale, C. A. Bader, A. Sorvina, K. D. M. MaGee, B. W. Skelton, T. A. Gillam, P. J. Wright, P. Raiteri, S. Stagni, J. L. Morrison, S. E. Plush, D. A. Brooks and M. Massi, *Chem. - Eur. J.*, 2017, **23**, 15666–15679.
- 20 V. Guerschais and J. L. Fillaut, *Coord. Chem. Rev.*, 2011, **255**, 2448–2457.
- 21 M. Keefe, K. D. Benkstein and J. T. Hupp, *Coord. Chem. Rev.*, 2000, **205**, 201–228.
- 22 J. Luo, Z. Xie, J. W. Y. Lam, L. Cheng, B. Z. Tang, H. Chen, C. Qiu, H. S. Kwok, X. Zhan, Y. Liu and D. Zhu, *Chem. Commun.*, 2001, **381**, 1740–1741.
- 23 R. Hu, N. L. C. Leung and B. Z. Tang, *Chem. Soc. Rev.*, 2014, **43**, 4494–4562.
- 24 Y. Hong, J. W. Y. Lam and B. Z. Tang, *Chem. Soc. Rev.*, 2011, **40**, 5361–5388.
- 25 J. Mei, N. L. C. Leung, R. T. K. Kwok, J. W. Y. Lam and B. Z. Tang, *Chem. Rev.*, 2015, **115**, 11718–11940.
- 26 Y. Liu, C. Deng, L. Tang, A. Qin, R. Hu, J. Z. Sun and B. Z. Tang, *J. Am. Chem. Soc.*, 2011, **133**, 660–663.
- 27 Y. Hong, J. W. Y. Lam and B. Z. Tang, *Chem. Commun.*, 2009, **29**, 4332–4353.
- 28 W. Lu, B. X. Mi, M. C. W. Chan, Z. Hui, C. M. Che, N. Zhu and S. T. Lee, *J. Am. Chem. Soc.*, 2004, **126**, 4958–4971.
- 29 Y. Sun, K. Ye, H. Zhang, J. Zhang, L. Zhao, B. Li, G. Yang, B. Yang, Y. Wang, S. W. Lai and C. M. Che, *Angew. Chemie - Int. Ed.*, 2006, **45**, 5610–5613.
- 30 V. W. W. Yam, K. H. Y. Chan, K. M. C. Wong and B. W. K. Chu, *Angew. Chemie - Int. Ed.*, 2006, **45**, 6169–6173.
- 31 Q. Zhao, L. Li, F. Li, M. Yu, Z. Liu, T. Yi and C. Huang, *Chem. Commun.*, 2008, **3**, 685–687.
- 32 B. H. Wu, M. J. Huang, C. C. Lai, C. H. Cheng and I. C. Chen, *Inorg. Chem.*, 2018, **57**, 4448–4455.
- 33 L. L. Wen, X. G. Hou, G. G. Shan, W. L. Song, S. R. Zhang, H. Z. Sun and Z. M. Su, *J. Mater. Chem. C*, 2017, **5**, 10847–10854.
- 34 C. Climent, P. Alam, S. S. Pasha, G. Kaur, A. R. Choudhury, I. R. Laskar, P. Alemany and D. Casanova, *J. Mater. Chem. C*, 2017, **5**, 7784–7798.
- 35 P. Alam, S. Dash, C. Climent, G. Kaur, A. R. Choudhury, D. Casanova, P. Alemany, R. Chowdhury and I. R. Laskar, *RSC Adv.*, 2017, **7**, 5642–5648.
- 36 G. Li, W. Guan, S. Du, D. Zhu, G. Shan, X. Zhu, L. Yan, Z. Su, M. R. Bryce and A. P. Monkman, *Chem. Commun.*, 2015, **51**, 16924–16927.
- 37 M. Mauro and C. Cebrían, *Isr. J. Chem.*, 2018, **58**, 901–914.
- 38 C. H. Shin, J. O. Huh, M. H. Lee and Y. Do, *Dalton Trans.*, 2009, **33**, 6476–9.
- Z. Song, R. Liu, Y. Li, H. Shi, J. Hu, X. Cai and H. Zhu, *J. Mater. Chem. C*, 2016, **4**, 2553–2559.
- 40 P. Alam, G. Kaur, A. Sarmah, R. K. Roy, A. R. Choudhury and I. R. Laskar, *Organometallics*, 2015, **34**, 4480–4490.
- 41 B. L. Reid, S. Stagni, J. M. Malicka, M. Cocchi, G. S. Hanan, M. I. Ogden and M. Massi, *Chem. Commun.*, 2014, **50**, 11580–11582.
- 42 X. Gu, T. Fei, H. Zhang, H. Xu, B. Yang, Y. Ma and X. Liu, *Eur. J. Inorg. Chem.*, 2009, **16**, 2407–2414.
- 43 L. Abad Galán, B. L. Reid, S. Stagni, A. N. Sobolev, B. W. Skelton, M. Cocchi, J. M. Malicka, E. Zysman-colman, E. G. Moore, M. I. Ogden and M. Massi, *Inorg. Chem.*, 2017, **56**, 8975–8985.
- 44 L. Abad Galán, A. N. Sobolev, B. W. Skelton, E. Zysman-colman, I. Mark and M. Massi, *ChemRxiv.*, 2018, 10.26434/chemrxiv.6008294.v1.
- 45 S. Lamansky, P. Djurovich, D. Murphy, F. Abdel-Razzaq, H. E. Lee, C. Adachi, P. E. Burrows, S. R. Forrest and M. E. Thompson, *J. Am. Chem. Soc.*, 2001, **123**, 4304–4312.
- 46 S. Lamansky, P. Djurovich, D. Murphy, F. Abdel-Razzaq, R. Kwong, I. Tsyba, M. Bortz, B. Mui, R. Bau and M. E. Thompson, *Inorg. Chem.*, 2001, **40**, 1704–1711.
- 47 A. P. Bassett, S. W. Magennis, P. B. Glover, D. J. Lewis, N. Spencer, S. Parsons, R. M. Williams, L. De Cola and Z. Pikramenou, *J. Am. Chem. Soc.*, 2004, **126**, 9413–9424.
- 48 V. V. Pavlishchuk and A. W. Addison, *Inorg. Chim. Acta*, 2000, **298**, 97–102.
- 49 K. Dedeian, J. Shi, N. Shepherd, E. Forsythe and D. C. Morton, *Inorg. Chem.*, 2005, **44**, 4445–4447.
- 50 E. Baranoff, B. F. E. Curchod, J. Frey, R. Scopelliti, F. Kessler, I. Tavernelli, U. Rothlisberger, M. Grätzel and M. K. Nazeeruddin, *Inorg. Chem.*, 2012, **51**, 215–224.
- 51 M. A. Halcrow and G. Christou, *Biomimetic Chemistry of Nickel*, 1994, vol. 94.
- 52 R. T. Jonas and T. D. P. Stack, *Inorg. Chem.*, 1998, **37**, 6615–6629.
- 53 Y. Wang, P. Bao, J. Wang, R. Jia, F. Bai and H. Zhang, *Inorg. Chem.*, 2018, **57**, 6561–6570.
- 54 A. Marini, A. Mun, A. Biancardi and B. Mennucci, *J. Phys. Chem. B*, 2010, **114**, 17128–17135.
- 55 J. M. Fernández-Hernández, J. I. Beltrán, V. Lemaure, M. D. Gálvez-López, C. H. Chien, F. Polo, E. Orsell, R. Fröhlich, J. Cornil and L. De Cola, *Inorg. Chem.*, 2013, **52**, 1812–1824.
- 56 A. Onder, M. Turkyilmaz and Y. Baran, *Inorg. Chim. Acta*, 2012, **391**, 28–35.
- 57 M. A. Chagas and W. R. Rocha, *Chem. Phys. Lett.*, 2014, **612**, 78–83.
- 58 J. Jayabharathi, V. Thanikachalam, N. Srinivasan and M. V. Perumal, *J. Fluoresc.*, 2011, **21**, 1585–1597.
- 59 S. Fantacci, F. De Angelis and A. Selloni, *J. Am. Chem. Soc.*, 2003, **125**, 4381–4387.
- 60 D. Chen, K. Li, X. Guan, G. Cheng, C. Yang and C. M. Che, *Organometallics*, 2017, **36**, 1331–1344.
- 61 K. Suzuki, A. Kobayashi, S. Kaneko, K. Takehira, T. Yoshihara, H. Ishida, Y. Shiina, S. Oishi and S. Tobita, *Phys. Chem. Chem. Phys.*, 2009, **11**, 9850.
- 62 A. J. Howarth, R. Patia, D. L. Davies, F. Lejl, M. O. Wolf and K. Singh, *Eur. J. Inorg. Chem.*, 2014, 3657–3664.
- 63 Y. Jiang, G. Li, W. Che, Y. Liu, B. Xu, G. Shan, D. Zhu, Z. Su and M. R. Bryce, *Chem. Commun.*, 2017, **53**, 3022–3025.
- 64 Q. Lu, X. Li, J. Li, Z. Yang, B. Xu, Z. Chi, J. Xu and Y. Zhang, *J. Mater. Chem. C*, 2015, **3**, 1225–1234.
- 65 G. a. Crosby and J. N. Demas, *J. Phys. Chem.*, 1971, **75**, 991–1024.
- 66 J. C. De Mello, H. F. Wittmann and R. H. Friend, *Adv. Mater.*, 1997, **9**, 230–232.
- 67 M. J. Frisch, G. W. Trucks, H. B. Schlegel, G. E. Scuseria,

- M. A. Robb, J. R. Cheeseman, G. Scalmani, V. Barone, G. A. Petersson, H. Nakatsuji, X. Li, M. Caricato, A. V. Marenich, J. Bloino, B. G. Janesko, R. Gomperts, B. Mennucci and J. B. Hratch, 2016.
- 68 Y. Zhao and D. G. Truhlar, *Theor. Chem. Acc.*, 2008, **120**, 215–241.
- 69 D. Jacquemin, E. A. Perpète, I. Ciofini, C. Adamo, R. Valero, Y. Zhao and D. G. Truhlar, *J. Chem. Theory Comput.*, 2010, **6**, 2071–2085.
- 70 D. Jacquemin, C. Adamo and B. Mennucci, *J. Chem. Theory Comput.*, 2012, **8**, 2359–2372.
- 71 J. Tomasi, B. Mennucci and R. Cammi, *Chem. Rev.*, 2005, **105**, 2999–3093.
- 72 Z. He, X. Qi, Z. She, Y. Zhao, S. Li, J. Tang, G. Gao, Y. Lan and J. You, *J. Org. Chem.*, 2017, **82**, 1403–1411.
- 73 C. H. Chang, Z. J. Wu, C. H. Chiu, Y. H. Liang, Y. S. Tsai, J. L. Liao, Y. Chi, H. Y. Hsieh, T. Y. Kuo, G. H. Lee, H. A. Pan, P. T. Chou, J. S. Lin and M. R. Tseng, *ACS Appl. Mater. Interfaces*, 2013, **5**, 7341–7351.
- 74 M. Nonoyama, *Bull. Chem. Soc. Jpn.*, 1974, **47**, 767–768.
- 75 2015.
- 76 P. T. Beurskens, G. Beurskens, R. de Gelder, S. Garcia-Granda, R. Israel and J. M. Smits, *M.DIRDIF-99*, The DIRDIF99 Program System, Technical Report of the University of Nijmegen, The Netherlands, 1999.
- 77 G. M. Sheldrick, *Acta Crystallogr. Sect. C Struct. Chem.*, 2015, **71**, 3–8.
- 78 2018.

The structural and photophysical properties of neutral Ir(III) complexes using modified  $\beta$ -diketonates as ancillary ligands have been investigated, resulting in significantly modulated aggregation induced emission properties.

**Key Topic\****AIE properties***Page No. – Page No.****Analyzing the Relation Between Structure and Aggregation Induced Emission (AIE) Properties of Iridium(III) Complexes through Modification of Non-Chromophoric Ancillary Ligands**